



Direct observation of entangled electronic-nuclear wave packets

Gönenç Moğol, Brian Kaufman , and Thomas Weinacht*

Department of Physics and Astronomy, Stony Brook University, Stony Brook New York 11794-3800, USA

Chuan Cheng 

Stanford PULSE Institute, SLAC National Accelerator Laboratory, Menlo Park, California 94025, USA
and Department of Physics and Astronomy, Stony Brook University, Stony Brook New York 11794-3800, USA

Itzik Ben-Itzhak 

James R. McDonald Laboratory, Kansas State University, Manhattan Kansas 66506-2604, USA



(Received 19 November 2023; accepted 23 April 2024; published 28 May 2024)

We present momentum resolved covariance measurements of entangled electronic-nuclear wave packets created and probed with octave spanning phaselocked ultrafast pulses. We launch vibrational wave packets on multiple electronic states via multiphoton absorption, and probe these wave packets via strong field double ionization using a second phaselocked pulse. Momentum resolved covariance mapping of the fragment ions highlights the nuclear motion, while measurements of the yield as a function of the relative phase between pump and probe pulses highlight the electronic coherence. The combined measurements allow us to directly visualize the entanglement between the electronic and nuclear degrees of freedom and follow the evolution of the complete wavefunction.

DOI: [10.1103/PhysRevResearch.6.L022047](https://doi.org/10.1103/PhysRevResearch.6.L022047)

Introduction. The interplay between electronic and nuclear dynamics is at the forefront of attosecond science and of fundamental importance for understanding energy flow at the molecular level [1–5]. Of particular interest is the role that electronic coherences play in driving basic photophysical processes such as photoisomerization, light harvesting, and how these coherences are affected by nuclear dynamics [6,7]. While electronic coherences in atoms can last for several nanoseconds and have been studied extensively [8–10], measurements of coherences in large molecules have been limited to a few femtoseconds [11–18], or in special cases a few tens of femtoseconds [19,22].

The rapid loss of electronic coherence is driven by the coupling between the electrons and the nuclei. This can be seen by writing the full molecular wave function after photo excitation in a Born-Huang (Oppenheimer) expansion:

$$\Psi(\mathbf{r}, \mathbf{R}, t) = a_1(t)\chi_1(\mathbf{R}, t)\psi_1(\mathbf{r}; \mathbf{R})e^{-i\omega_1(\mathbf{R})t} + a_2(t)\chi_2(\mathbf{R}, t)\psi_2(\mathbf{r}; \mathbf{R})e^{-i\omega_2(\mathbf{R})t} + \dots, \quad (1)$$

where ψ_i represents the i th electronic state of the molecule and χ_i represents the nuclear wavefunction on the i th

electronic state. The frequencies in the exponent ω_i are defined by the formula $\omega_i(\mathbf{R}) = V_i(\mathbf{R})/\hbar$, where $V_i(\mathbf{R})$ is the potential energy surface of state i as a function of the nuclear coordinate \mathbf{R} . The coefficients a_i can depend on time because internal conversion or intersystem crossing can lead to a changes in the population of a given electronic state; however, this is not relevant in this experiment.

The wave packet described by Eq. (1) can be created by multiphoton absorption using a very short (~ 2 cycle) pulse [20], such that the excitation is dominated by a single subcycle of the pulse. In the case of n -photon absorption, the effective bandwidth of the n th order Rabi frequency is \sqrt{n} times the spectral bandwidth, allowing for excitation of multiple electronic states for any given photon order. When driving n -photon absorption, it is natural to expect $n \pm 1$ order excitation of nearby states [20–22].

Here we focus on the special case of Eq. (1) for two excited states which are separated by one photon order (e.g., four and five photon absorption). The off diagonal term of the density matrix, which expresses the electronic coherence, is given by

$$\rho_{12}(\mathbf{R}, t) = a_1\chi_1(\mathbf{R}, t)a_2^*\chi_2^*(\mathbf{R}, t)e^{i(\omega_2(\mathbf{R})-\omega_1(\mathbf{R}))t} \quad (2)$$

In our experiment we are considering an n -photon absorption to the state 1, and $(n+1)$ -photon absorption to state 2 by the pump pulse, which we can write as $E_{\text{pu}}(t) = E_0(t)\cos(\omega_0 t)$. Subsequently, a probe pulse doubly ionizes both excited states with m -photon and $(m-1)$ -photon absorption, respectively. Double ionization is established by velocity map imaging measurements of fragment ions in covariance [23,24]. The pump and the probe pulses are phase locked and the probe pulse is delayed by τ , so we can write the

*Author to whom correspondence should be addressed: thomas.weinacht@stonybrook.edu

Published by the American Physical Society under the terms of the Creative Commons Attribution 4.0 International license. Further distribution of this work must maintain attribution to the author(s) and the published article's title, journal citation, and DOI.

electric field as $E_{\text{pr}}(t) = E'_0(t - \tau) \cos(\omega_0(t - \tau) - \phi)$, where we control the phase ϕ and delay τ with our pulse shaper. Making use of the expression for $\rho_{12}(\mathbf{R}, t)$ given above, we can express the dication yield as

$$Y(\mathbf{R}, t) = |a_1|^2 |b_1|^2 + |a_2|^2 |b_2|^2 + b_1 b_2^* \rho_{12}(\mathbf{R}, t) + \text{c.c.} \quad (3)$$

Here, b_1 and b_2 represent the ionization amplitudes for states 1 and 2, which are proportional to the m th and $(m - 1)$ th power of the electric field of the probe:

$$b_1(t) = Q_{1f}(E_{\text{pr}}(t))^m \quad (4a)$$

$$b_2(t) = Q_{2f}(E_{\text{pr}}(t))^{(m-1)}, \quad (4b)$$

where Q_{1f} and Q_{2f} are the matrix elements for ionization from state 1 or 2, respectively, into the final dicationic state f . Integrating over t , one can arrive at an expression for the ionization yield in terms of the delay τ and phase ϕ that we control [25]:

$$Y(\mathbf{R}, \tau, \phi) = |a_1|^2 |Q_{1f}(E'_0)^m|^2 + |a_2|^2 |Q_{2f}(E'_0)^{m-1}|^2 + a_1 a_2^* Q_{1f} Q_{2f}^* (E'_0)^{(2m-1)} e^{i\phi} \rho_{12}(\mathbf{R}, \tau) + \text{c.c.} \quad (5)$$

This expression highlights the phase dependence of the ionization yield and three mechanisms for electronic decoherence. The first is the loss of wavefunction overlap—the decay of the product $\chi_1(\mathbf{R}, \tau) \chi_2^*(\mathbf{R}, \tau)$. The second is dephasing—an \mathbf{R} dependent phase advance $\omega_2(\mathbf{R}) - \omega_1(\mathbf{R})$, which washes out the \mathbf{R} integrated yield. The last is the loss of population, i.e., the decay of the coefficients a_i via internal conversion or intersystem crossings. All three contributions to decoherence can be suppressed for states with parallel potential energy surfaces, which can minimize internal conversion and dephasing, and for which the wave packet evolution is very similar, maintaining the overlap. Furthermore, if one is able to perform \mathbf{R} -resolved measurements, then one can further mitigate dephasing since one limits the range in \mathbf{R} over which the phase term is integrated. Here, we experimentally demonstrate long lived electronic coherences between dissociative states of a polyatomic molecule with parallel potential energy surfaces, and illustrate how covariance velocity map imaging of the fragment ions arising from the dication (providing KER resolved measurements) allows us to directly view the entangled electronic and nuclear degrees of freedom, which leads to dephasing and the decay of electronic coherence.

There have been many studies that aim to determine the dominant mechanism for the loss of coherence [3,17,19,26–30]. While the dominant mechanism can depend on the details of the molecular system, calculations support the idea that vibrational dephasing can be mitigated in states with parallel potentials, leading to long lasting coherences [27].

In earlier work [22], we found parallel potentials for relatively low-lying states of the molecule Thiophene—states involving excitation of lone pair orbitals. Here we consider excitation of high lying Rydberg states, for which the potential energy surfaces are approximately parallel [22,31].

In this paper we study entangled nuclear-electronic wave packets in 1,1,1-Trifluoroacetone (3F-acetone), which has the chemical formula CF_3COCH_3 . Via multiphoton excitation, we excite the molecule to a pair of high-lying Rydberg states

of the neutral molecule. We then follow the evolution of electronic coherences between these two states and demonstrate how electronic coherences can be maintained even in the face of large amplitude nuclear motion (i.e., dissociation).

Experimental Method. We carried out measurements using a commercial amplified titanium sapphire laser that produces 30-fs pulses at 1 kHz with up to 1-mJ pulse energy. The 30-fs pulses are spectrally broadened using an Argon-filled 2.1-m long hollow-core fiber with inner diameter of 450 μm (see Fig. 5 in the Appendix for the spectrum). The broadened pulses are then compressed and shaped using an acousto-optic modulator (AOM) pulse shaper [32].

The initial electric field $E(\nu)$ is shaped in the frequency domain (at the Fourier plane of the pulse shaper) by an acoustic mask $M(\nu)$ programed onto the AOM to produce a pump-probe pulse pair. The shaped electric field $\tilde{E}(\nu)$ is given by $\tilde{E}(\nu) = M(\nu)E(\nu)$. For control of the pump-probe delay and relative phase between the pulses, we choose a mask of the form

$$M(\nu) = A_{\text{tot}}(1 + A_R \exp(i2\pi\tau(\nu - \nu_L) + i\phi_L)), \quad (6)$$

where A_{tot} controls the overall amplitude, R the relative amplitude ($E'_0 = A_R E_0$), ϕ_L the relative phase, and τ the relative delay between the two pulses. The quantity ν_L is the locking frequency and writes a delay dependent relative phase such that there is always constructive interference at the frequency ν_L (for $\phi_L = 0$), regardless of the delay between the two pulses. Thus, the controllable phase of the laser can be described by $\phi = \phi_L - 2\pi\nu_L\tau$.

In addition to control of the pulse pair, the pulse shaper also allows us to characterize the pulses we generate. We perform pulse-shaper-assisted, second harmonic generation collinear frequency resolved optical gating (PS-CFROG) to determine the temporal profile of our pulses [32]. The resulting compressed and shaped pulses have a minimum duration of 7 fs FWHM (see Fig. 5 in the Appendix). We made extensive use of the AOM pulse shaping capability to compress, control, and characterize the laser pulses [32].

The shaped pulses are focused onto an effusive molecular beam of 3F-acetone inside the velocity map imaging spectrometer using a 5 cm focal length concave silver mirror, which is inside the vacuum chamber. The base pressure of the vacuum chamber is 10^{-10} Torr. The molecule 3F-acetone is introduced into a separate sample chamber, and then skimmed into the reaction chamber in order to yield an effusive beam. This effusive beam overlaps with the laser focus at the center of our VMI apparatus. The partial pressure of 3F-acetone inside the reaction chamber was kept around 5×10^{-8} Torr in order to yield the desired count rate of around 5–10 ion hits per laser shot.

We collect ion momentum data using a velocity map imaging system, which has funnel microchannel plates with open area of $\sim 90\%$ and a P47 phosphor screen (depicted schematically in Fig. 1). The hits are recorded by a Timepix camera, whose pixels have a time of arrival resolution of 1.5 ns [33,34], allowing us to simultaneously record and resolve all of the fragment ions produced in a given laser shot. Furthermore, the Timepix camera allows us to reconstruct the 3D momentum of ions using the time of flight of ions and their

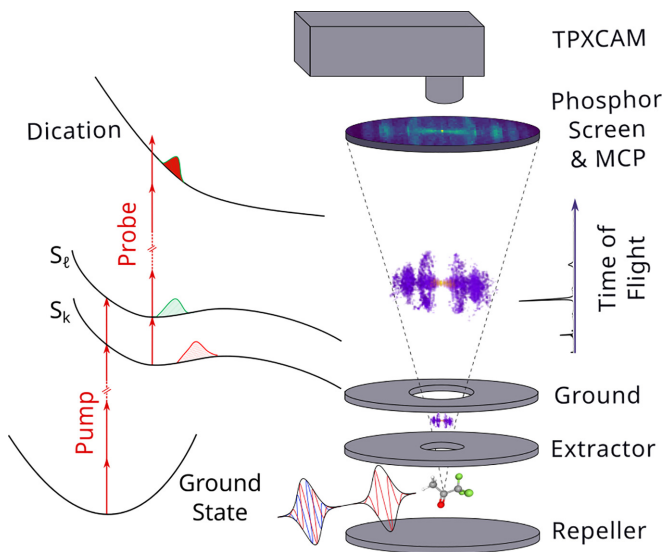


FIG. 1. Left panel: Potential energy curves and excitation scheme for detecting electronic coherences. The molecule is excited to a pair of high-lying Rydberg states that are separated by one photon energy and then doubly ionized with a probe pulse. Right panel: Shaped, phaselocked pump and probe pulses with velocity map imaging apparatus for phase sensitive KER resolved measurements of fragments from molecular dications.

position $([x, y, t] \mapsto [p_x, p_y, p_z])$ without the need for Abel inversion [34,35]. We estimate the peak laser intensity for an unshaped laser pulse at the focus to be 550 TW/cm^2 (corresponding to individual pump and probe intensities of about 230 TW/cm^2 and 550 TW/cm^2 , respectively), which we have obtained from the $2U_p$ cutoff of above-threshold ionization of Argon.

Results. We measured the momenta of fragment ions from 3F-acetone in covariance as a function of the delay and the relative phase between the two pulses. We focus on the fragmentation of the molecule along the $\text{CF}_3 - \text{COCH}_3$ bond using covariance velocity map imaging. In particular, we look at the correlation of CF_3^+ and COCH_3^+ ions in the dataset on a shot by shot basis, which allows us to hone in on the dissociation along the $\text{CF}_3 - \text{COCH}_3$ coordinate. Working in covariance provides the same information as coincidence, but allows us to work in a higher count rate regime [23,24,36,37].

In Fig. 2 we present the results of the pump-probe measurements, which show the energy resolved covariance yield of CF_3^+ and COCH_3^+ ions as a function of the pump-probe delay for a locking frequency $\omega_L = 2.51 \times 10^{15} \text{ rad/s}$, which corresponds to a central wavelength of 750 nm. Measuring these two fragment ions in covariance and checking for momentum conservation confirms that they come from the same molecular dication, and allows us to draw some simple conclusions about the dynamics between pump and probe pulses. There are two prominent features in Fig. 2: the kinetic energy release decreases with pump-probe delay, and the covariance yield is modulated with a period of $33 \pm 5 \text{ fs}$. The monotonic decrease in kinetic energy release with pump-probe delay is consistent with dissociation along this bond, while the modulations in the yield are consistent with vibrations during dissociation.

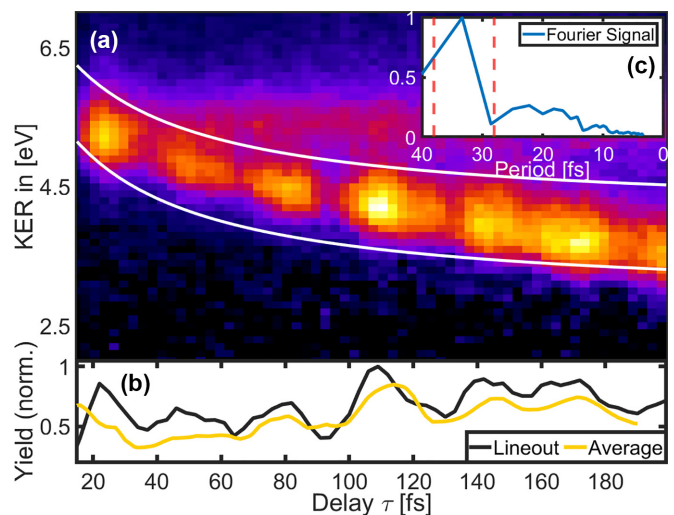


FIG. 2. (a) Kinetic energy release (KER) resolved covariance between CF_3^+ and COCH_3^+ ions as a function of pump-probe delay. The y axis shows the total KER from these ions and the x axis represents the pump-probe delay. (b) is the yield integrated between the two white lines (black), as well as the yield averaged over all locking frequencies (yellow). Inset: Fourier analysis of the locking frequency averaged yield.

As the KER resolved pump-probe measurements of the fragment ions point toward dissociative dynamics, we considered electronic states of both the neutral and monocation. The ground state of the monocation is dissociative along the $\text{COCH}_3^+ - \text{CF}_3$ coordinate [38,39], meaning that the dynamics could take place on low lying states of the cation or high lying Rydberg states of the neutral, which are parallel to the lowest cationic state. We argue below based on phase dependent measurements that it is unlikely to be cationic states.

In order to interpret the modulations in the covariance yield, we calculated the vibrational frequencies of the neutral ground state at the B3LYP level of theory. The modes with frequencies near the measured modulation frequency are listed in (Table I) of the Appendix. Given that we expect the electronically excited states of the molecule to have slightly lower frequencies than the ground state, and that the modulations have a pronounced effect on the CF_3^+ and COCH_3^+ yield, we suspect that it is the antisymmetric CF_3 stretch mode of the molecule which underlies the modulations in the measured yields. Note that this mode involves not just a vibration of the CF_3 group, but all of the other atoms in the molecule as well [40]. In Fig. 7 in the Appendix we depict the motion

TABLE I. Various vibrational excitations of 3F-acetone which have a period around $33 \pm 5 \text{ fs}$ at the Frank-Condon point of the ground state calculated at B3LYP level of theory.

Assignment [42]	Frequency [cm^{-1}]	Period [fs]
CH_3 symmetric rock	962	35
CH_3 antisymmetric rock	1027	32
CF_3 symmetric stretch	1131	29
CF_3 antisymmetric stretch	1189	28

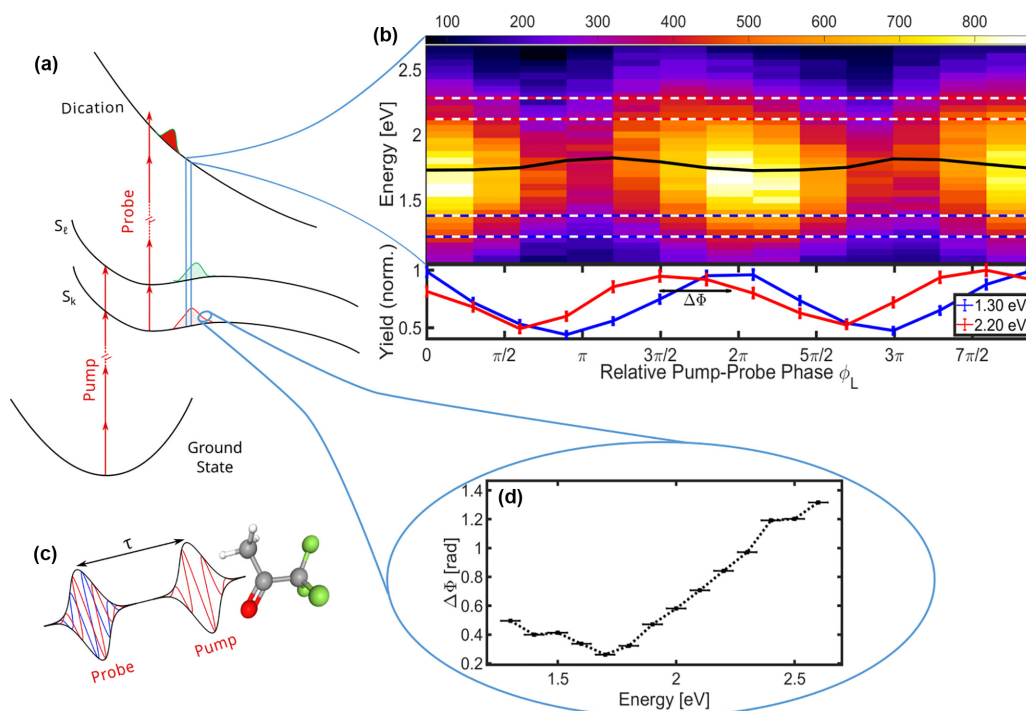


FIG. 3. Measurement scheme with CF_3^+ energy and phase dependent yield. (a) Potential energy curves for states relevant to the creation and detection of a coupled electron-nuclear wave packet. (b) CF_3^+ double ionization yield as a function of CF_3^+ energy and pump-probe delay with lineouts below for two different energy regions as well as the center of mass of the distribution in black. (c) Schematic of shaped, phaselocked pump and probe pulses with different relative phases. (d) Phase extracted from fitting the data in panel (b) as a function of CF_3^+ energy.

of this antisymmetric CF_3 mode that we associate with the modulations seen in Fig. 2.

With the pulse shaper, we have the ability to perform pump-probe measurements with independent control over the phase and delay between pump and probe pulses. This allows us to confirm that the modulations in the covariance yield arise from a vibrational coherence rather than an electronic one. The bottom panel of Fig. 2 compares the measurements carried out for a fixed phase between pump and probe pulses with measurements that are averaged over all phases at each delay. Both measurements show clear modulations in the yield, consistent with these arising from vibrations which modulate the ionization yield.

While pump-probe measurements which average over phase allow us to focus on vibrational dynamics, phase scans at fixed delays highlight electronic coherences, as shown in Fig. 5. In Fig. 3 we present the phase scan at a fixed delay of 95 fs. We chose this delay partially to rule out any optical interference between the pump and the probe pulses, and partially to highlight the long lived electronic coherences which persist during dissociation. In the Appendix we detail how we have ruled out optical interference of the two pulses. Since we see a single modulation of the energy resolved yield in Fig. 3 within 2π phase, as opposed to multiple modulations within 2π , the states that contribute to the electronic coherence must be separated by a single photon energy [41].

Single point electronic structure calculations at the Frank-Condon point for the ion show that there are no pairs of states of the cation that are separated by a single photon. We thus conclude that the electronic coherence is coming from high-lying states of the neutral molecule. The fact that the

states are high lying also has the consequence that the potential energy surfaces are likely close to being parallel to each other [22,31]. This effect decreases the decoherence of the two states due to loss of wave function overlap as outlined in the introduction.

Figure 3 shows an explicit manifestation of entanglement between nuclear and electronic degrees of freedom. Here we plot the energy resolved yield of the CF_3^+ fragment, instead of the covariant kinetic energy release from CF_3^+ and COCH_3^+ since the statistics are better for the single fragment yield. We have, however, used the covariance method to confirm that the plotted yield is indeed coming from the dissociation along the $\text{CF}_3 - \text{COCH}_3$ bond. Note that the kinetic energy of the CF_3^+ fragment is determined by the $\text{CF}_3 - \text{COCH}_3$ distance. As the kinetic energy of the CF_3^+ changes, so does the position of constructive interference of the two wave packets. This is highlighted by the variation in the first moment of the energy distribution, which is plotted in black on top of the 2D color plot. We make this connection explicit by plotting in panel (d) the phase shift, $\Delta\Phi$, between the different lineouts [black arrow shown with the red and blue curves in the bottom of panel (b)] from Fig. 3 as a function of kinetic energy of the CF_3^+ fragment. This nontrivial correlation between the relative phase and the kinetic energy of the CF_3^+ fragment implies that the measured yield cannot be expressed as a product of functions of KER and phase, and therefore that the molecular wave function cannot be written as a product of functions of electronic and nuclear degrees of freedom. In this sense we interpret the modulations in Fig. 3 as direct signature of the entanglement between electronic and nuclear degrees of freedom.

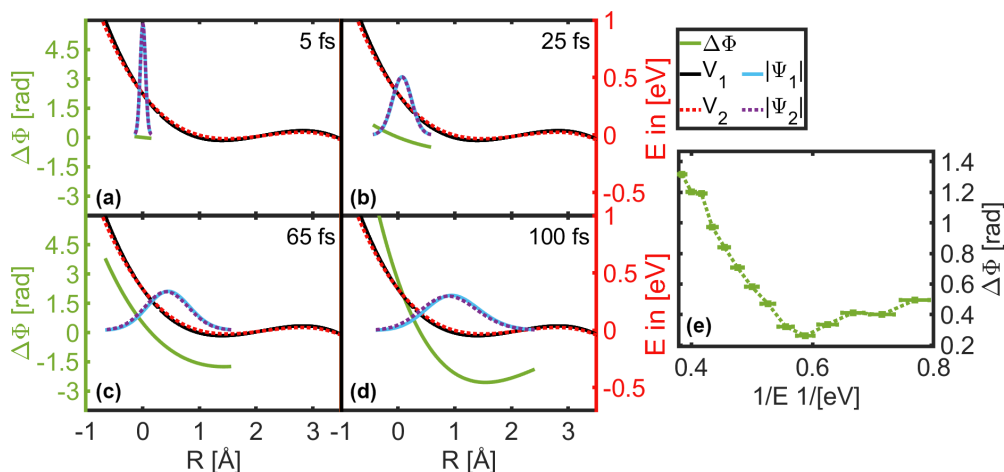


FIG. 4. [(a)–(d)] Time evolution of two wave packets on slightly different dissociative potentials. In green is the R -dependent phase difference between the wavefunctions. The wavefunctions are scaled for easier viewing. (e) Replot of the experimental phase scan from panel (d) of Fig. 3. The x axis is converted into $1/E$ to represent R because of the Coloumb potential relation $E \sim 1/R$.

As a test of the basic idea that our measurements are sensitive to the KER dependent (and thus the R coordinate dependent) phase difference between the wavefunctions on the two electronic states, we carried out calculations where we solve the time dependent Schrödinger equation (TDSE) for a model 1D potential. We consider two wave packets propagating on slightly different parallel potentials. We employ the split operator formalism to propagate the initial wavefunctions on the two dissociative potentials and plot the evolution of the phase difference between the two wavefunctions. Fig. 4 shows the results of the calculations. We see a qualitative agreement between the measured phase difference and the phase difference of two wavefunctions. The potential used in the calculations is based on our expectation for the high lying Rydberg states of the molecule, which are parallel to the ground state of the molecular cation [31,38]. We defined the potential in the calculations as a cubic spline between four points, roughly setting the position of the initial roll down, the minimum, the barrier height, and the roll down after the barrier. We fixed these four points and generated a

series of potentials by randomly varying around these points in order to determine the sensitivity of the calculations to the details of the potential energy curve on which the wave packets evolve. Our calculations showed the same qualitative features independent of the exact shape of the potential: As shown in panel (a), the wave packets initially have very little phase difference because they haven't propagated on the potentials for enough time to develop a phase difference. As the wave packets pick up momentum on slightly different potentials, we see a linear phase difference between them (b). As the wave packets further progress down the potential and experience less acceleration or are slowed down by the barrier, the linear phase difference evolves into a hockey stick shaped feature (c) and (d). We have confirmed that this hockey stick shaped feature in panel (c) persists qualitatively as we vary the potentials around the fixed points. We have further replotted the experimental measurements from 3(d) to 4(e). We changed the x -axis from E to $1/E$ to approximately calibrate an energy to internuclear distance à la Coulomb's law to ease the comparison of experimental measurements with the 1D model. This comparison furthers our interpretation that the measurements we show in Fig. 3 are indeed resulting from the coherent interference of two wave packets

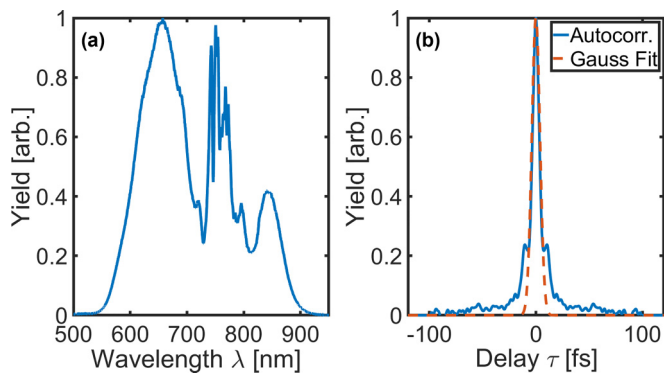


FIG. 5. (a) Spectrum of the laser pulses out of the hollow-core fiber. The spectrum is structured, consistent with self-phase modulation in hollow-core fibers. (b) Intensity cross correlation signal from CFROG and the Gaussian fit to it. Note that the FWHM is 7 fs and there are no pre or post pulses at large delays.

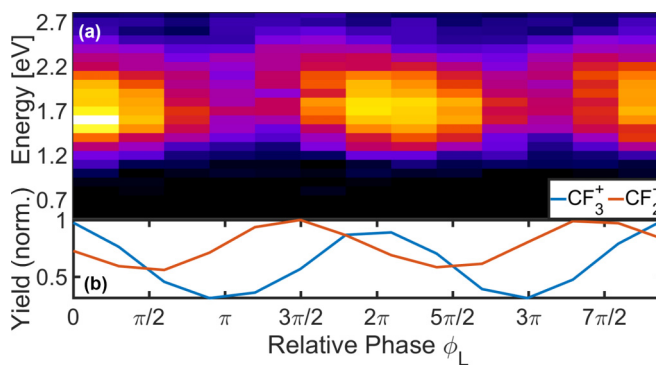


FIG. 6. (a) Energy resolved yield of CF_3^+ in covariance with $COCH_3^+$ ion. (b) Marginal of the above covariance yield (blue) and marginal of the yield of CF_2^+ .

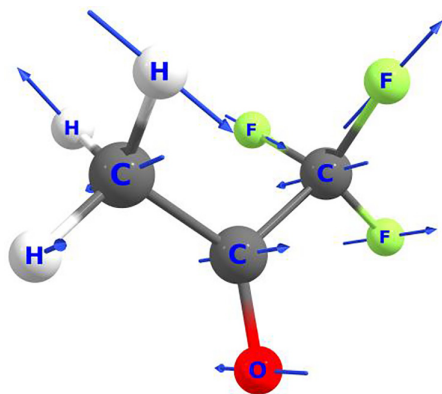


FIG. 7. Displacement vectors for antisymmetric stretch of CF_3 .

propagating on approximately parallel dissociative potential energy surfaces.

Conclusion. In conclusion, we have presented measurements of entangled nuclear-electronic wave packet dynamics in a multimode molecular system. In particular, we have observed a pump-probe phase dependence of the energy resolved yield of molecular fragments Fig. 3. A phase locked pump-probe pulse pair launches and interrogates the wave packet dynamics via multiphoton excitation and ionization. Fragment ions are measured with momentum resolved covariance velocity map imaging. In the pump-probe scan we observe a dissociation along the $\text{CF}_3 - \text{COCH}_3$ bond which is coupled with vibrational excitation of the molecule Fig. 2. Our measurements highlight the entanglement between electronic and nuclear degrees of freedom, and demonstrate the maintenance of electronic coherence despite large amplitude nuclear motion.

The data that support the findings of this study are available from the corresponding author upon reasonable request.

Acknowledgments. G.M., B.K., C.C., and T.C.W. were supported by the National Science Foundation under Award No. 2110376. I.B.I. was supported by the Chemical Sciences, Geosciences, and Biosciences Division, Office of Basic Energy Science, Office of Science, U.S. Department of Energy, under Award No. DE-FG02-86ER13491.

The authors declare that they have no conflicts of interest.

Appendix. We took care in ruling out any optical interference between the pump and the probe pulses. We checked for optical interference in two independent ways. The first was to perform detailed pulse characterization measurements, using PS-CFROG to characterize the pulses. In Fig. 5 we plot the spectrum and the CFROG of the compressed pulse. Note that while there is some structure in the pulse around 10 fs, there are no pre or post pulses at longer (~ 95 fs) delays where we carry out our interference measurements.

Our second independent check is looking at the phase dependence of different fragment ions. If optical interference were giving rise to the modulations seen in Fig. 3 it would be because the total electric field varies with phase as a result of constructive and destructive interference. In this case the phase dependence of the yields of all fragments in a given dataset would be the same because the modulations are only due to variation in the total intensity. This is, however, not the case as we show in Fig. 6. There we can see that the CF_3^+ and CF_2^+ yields are phase shifted relative to each other. Combined with our characterization of the pulses, we conclude that the phase variation is due to dynamics in the molecule and is not an optical interference effect.

- [1] P. B. Corkum and F. Krausz, Attosecond science, *Nat. Phys.* **3**, 381 (2007).
- [2] A. Palacios and F. Martín, The quantum chemistry of attosecond molecular science, *Wiley Interdiscip. Rev.: Comput. Mol. Sci.* **10**, e1430 (2020).
- [3] L.-M. Koll, L. Maikowski, L. Drescher, T. Witting, and M. J. J. Vrakking, Experimental control of quantum-mechanical entanglement in an attosecond pump-probe experiment, *Phys. Rev. Lett.* **128**, 043201 (2022).
- [4] M. J. J. Vrakking, Ion-photoelectron entanglement in photoionization with chirped laser pulses, *J. Phys. B* **55**, 134001 (2022).
- [5] M. J. J. Vrakking, Control of attosecond entanglement and coherence, *Phys. Rev. Lett.* **126**, 113203 (2021).
- [6] H.-G. Duan, V. I. Prokhorenko, R. J. Cogdell, K. Ashraf, A. L. Stevens, M. Thorwart, and R. J. D. Miller, Nature does not rely on long-lived electronic quantum coherence for photosynthetic energy transfer, *Proc. Natl. Acad. Sci.* **114**, 8493 (2017).
- [7] M. Maiuri, E. E. Ostroumov, R. G. Saer, R. E. Blankenship, and G. D. Scholes, Coherent wavepackets in the Fenna–Matthews–Olson complex are robust to excitonic-structure perturbations caused by mutagenesis, *Nat. Chem.* **10**, 177 (2018).
- [8] H. Maeda and T. F. Gallagher, Nondispersing wave packets, *Phys. Rev. Lett.* **92**, 133004 (2004).
- [9] T. C. Weinacht, J. Ahn, and P. H. Bucksbaum, Measurement of the amplitude and phase of a sculpted Rydberg wave packet, *Phys. Rev. Lett.* **80**, 5508 (1998).
- [10] J. A. Yeazell, M. Mallalieu, and C. R. Stroud, Observation of the collapse and revival of a Rydberg electronic wave packet, *Phys. Rev. Lett.* **64**, 2007 (1990).
- [11] C. Arnold, O. Vendrell, and R. Santra, Electronic decoherence following photoionization: Full quantum-dynamical treatment of the influence of nuclear motion, *Phys. Rev. A* **95**, 033425 (2017).
- [12] G. J. Halász, A. Perveaux, B. Lasorne, M. A. Robb, F. Gatti, and Á. Vibók, Coherence revival during the attosecond electronic and nuclear quantum photodynamics of the ozone molecule, *Phys. Rev. A* **88**, 023425 (2013).
- [13] I. Franco, M. Shapiro, and P. Brumer, Femtosecond dynamics and laser control of charge transport in trans-polyacetylene, *J. Chem. Phys.* **128**, 244905 (2008).
- [14] A. Scheidegger, J. Vaníček, and N. V. Golubev, Search for long-lasting electronic coherence using on-the-fly ab initio semiclassical dynamics, *J. Chem. Phys.* **156**, 034104 (2022).

- [15] H. Hwang and P. J. Rossky, Electronic decoherence induced by intramolecular vibrational motions in a betaine dye molecule, *J. Phys. Chem. B* **108**, 6723 (2004).
- [16] H. Kamisaka, S. V. Kilina, K. Yamashita, and O. V. Prezhdo, Ultrafast vibrationally-induced dephasing of electronic excitations in pbse quantum dots, *Nano Lett.* **6**, 2295 (2006).
- [17] M. Vacher, M. J. Bearpark, M. A. Robb, and J. P. Malhado, Electron dynamics upon ionization of polyatomic molecules: Coupling to quantum nuclear motion and decoherence, *Phys. Rev. Lett.* **118**, 083001 (2017).
- [18] M. Vacher, L. Steinberg, A. J. Jenkins, M. J. Bearpark, and M. A. Robb, Electron dynamics following photoionization: Decoherence due to the nuclear-wave-packet width, *Phys. Rev. A* **92**, 040502(R) (2015).
- [19] V. Despré, N. V. Golubev, and A. I. Kuleff, Charge migration in propiolic acid: A full quantum dynamical study, *Phys. Rev. Lett.* **121**, 203002 (2018).
- [20] B. Kaufman, P. Marquetand, T. Weinacht, and T. Rozgonyi, Numerical calculations of multiphoton molecular absorption, *Phys. Rev. A* **106**, 013111 (2022).
- [21] W. D. M. Lunden, P. Sándor, T. C. Weinacht, and T. Rozgonyi, Model for describing resonance-enhanced strong-field ionization with shaped ultrafast laser pulses, *Phys. Rev. A* **89**, 053403 (2014).
- [22] B. Kaufman, P. Marquetand, T. Rozgonyi, and T. Weinacht, Long-lived electronic coherences in molecules, *Phys. Rev. Lett.* **131**, 263202 (2023).
- [23] C. Cheng, L. J. Frasinski, G. Moğol, F. Allum, A. J. Howard, D. Rolles, P. H. Bucksbaum, M. Brouard, R. Forbes, and T. Weinacht, Multiparticle cumulant mapping for coulomb explosion imaging, *Phys. Rev. Lett.* **130**, 093001 (2023).
- [24] F. Allum, C. Cheng, A. J. Howard, P. H. Bucksbaum, M. Brouard, T. Weinacht, and R. Forbes, Multi-particle three-dimensional covariance imaging: “coincidence” insights into the many-body fragmentation of strong-field ionized D₂O, *J. Phys. Chem. Lett.* **12**, 8302 (2021).
- [25] B. Kaufman, P. Marquetand, T. Rozgonyi, and T. Weinacht, Long lived electronic coherences in molecular wave packets probed with pulse shape spectroscopy, *Phys. Rev. A* (2023).
- [26] D. T. Matselyukh, V. Despré, N. V. Golubev, A. I. Kuleff, and H. J. Wörner, Decoherence and revival in attosecond charge migration driven by non-adiabatic dynamics, *Nat. Phys.* **18**, 1206 (2022).
- [27] J. Vester, V. Despré, and A. I. Kuleff, The role of symmetric vibrational modes in the decoherence of correlation-driven charge migration, *J. Chem. Phys.* **158**, 104305 (2023).
- [28] D. Dey, A. I. Kuleff, and G. A. Worth, Quantum interference paves the way for long-lived electronic coherences, *Phys. Rev. Lett.* **129**, 173203 (2022).
- [29] M. Vacher, F. E. A. Albertani, A. J. Jenkins, I. Polyak, M. J. Bearpark, and M. A. Robb, Electron and nuclear dynamics following ionisation of modified bismethylene-adamantane, *Faraday Discuss.* **194**, 95 (2016).
- [30] A. Csehi, P. Badankó, G. J. Halasz, Á. Vibók, and B. Lasorne, On the preservation of coherence in the electronic wavepacket of a neutral and rigid polyatomic molecule, *J. Phys. B* **53**, 184005 (2020).
- [31] G. N. Gibson, R. R. Freeman, and T. J. McIlrath, Dynamics of the high-intensity multiphoton ionization of N₂, *Phys. Rev. Lett.* **67**, 1230 (1991).
- [32] A. Catanese, B. Kaufman, C. Cheng, E. Jones, M. G. Cohen, and T. Weinacht, Acousto-optic modulator pulse-shaper compression of octave-spanning pulses from a stretched hollow-core fiber, *OSA Continuum*. **4**, 3176 (2021).
- [33] A. Nomerotski, Imaging and time stamping of photons with nanosecond resolution in timepix based optical cameras, *Nucl. Instrum. Methods Phys. Res., Sect. A* **937**, 26 (2019).
- [34] C. Cheng, R. Forbes, A. J. Howard, M. Spanner, P. H. Bucksbaum, and T. Weinacht, Momentum-resolved above-threshold ionization of deuterated water, *Phys. Rev. A* **102**, 052813 (2020).
- [35] A. Zhao, M. van Beuzekom, B. Bouwens, D. Byelov, I. Chakaberia, C. Cheng, E. Maddox, A. Nomerotski, P. Svihra, J. Visser, V. Vrba, and T. Weinacht, Coincidence velocity map imaging using Tpx3Cam, a time stamping optical camera with 1.5 ns timing resolution, *Rev. Sci. Instrum.* **88**, 113104 (2017).
- [36] C. Cheng, V. Singh, S. Matsika, and T. Weinacht, Strong field double ionization of formaldehyde investigated using momentum resolved covariance imaging and trajectory surface hopping, *J. Phys. Chem. A* **126**, 7399 (2022).
- [37] A. E. Boguslavskiy, J. Mikosch, A. Gijsbertsen, M. Spanner, S. Patchkovskii, N. Gador, M. J. J. Vrakking, and A. Stolow, The multielectron ionization dynamics underlying attosecond strong-field spectroscopies, *Science* **335**, 1336 (2012).
- [38] D. Cardoza, M. Baertschy, and T. Weinacht, Understanding learning control of molecular fragmentation, *Chem. Phys. Lett.* **411**, 311 (2005).
- [39] D. Cardoza, M. Baertschy, and T. Weinacht, Interpreting closed-loop learning control of molecular fragmentation in terms of wave-packet dynamics and enhanced molecular ionization, *J. Chem. Phys.* **123**, 074315 (2005).
- [40] The naming convention comes from the prominent movement of the CF₃ group.
- [41] In general, if the states were separated by K photons we would see K modulations within 2π as the phase term in Eq. (5) would become $e^{iK\phi}$.
- [42] J. R. Durig and J. S. Church, Vibrational spectra and the assignment of the normal modes of 1,1,1-trifluoro-2-propanone, *Spectrochimica Acta Part A: Molecular Spectroscopy* **36**, 957 (1980).